Published in final edited form as:
Toxicol Sci. 2007 July ; 98(1): 249–257. doi:10.1093/toxsci/kfm074.

MIGRATION OF INTRADERMALLY INJECTED QUANTUM DOTS TO SENTINEL ORGANS IN MICE

Neera V. Gopee[a,b], **Dean W. Roberts**[a,b], **Peggy Webb**[a,b], **Christy R. Cozart**[a], **Paul H. Siitonen**[a], **Alan R. Warbritton**[c], **William W. Yu**[d], **Vicki L. Colvin**[d], **Nigel J. Walker**[e], and **Paul C. Howard**[a,b,*]

[a]National Center for Toxicological Research, U.S. Food & Drug Administration, Jefferson, AR 72079

[b]National Toxicology Program Center for Phototoxicology, U.S. Food & Drug Administration, Jefferson, AR 72079

[c]Toxicology Pathology Associates, Jefferson, AR 72079

[d]Center for Biological and Environmental Nanotechnology and Department of Chemistry, Rice University, Houston, TX

[e]National Institute of Environmental Health Sciences, National Institutes of Health, and the National Toxicology Program, Research Triangle Park, NC

Abstract

Topical exposure to nanoscale materials is likely from a variety of sources including sunscreens and cosmetics. Because the *in vivo* disposition of nanoscale materials is not well understood, we have evaluated the distribution of quantum dots (QD) following intradermal injection into female SKH-1 hairless mice as a model system for determining tissue localization following intradermal infiltration. The QD [CdSe core, CdS capped, poly(ethylene glycol) (PEG) coated, 37 nm diameter, 621 nm fluorescence emission] were injected intradermally on the right dorsal flank. Within minutes following intradermal injection, the highly UV fluorescent QD could be observed moving from the injection sites apparently through the lymphatic duct system to regional lymph nodes. Residual fluorescent QD remained at the site of injection until necropsy at 24 hours. Quantification of cadmium and selenium levels after 0, 4, 8, 12 or 24 hours in multiple tissues, using inductively coupled plasma mass spectrometry (ICP-MS) showed a time-dependent loss of cadmium from the injection site, and accumulation in the liver, regional draining lymph nodes, kidney, spleen, and hepatic lymph node. Fluorescence microscopy corroborated the ICP-MS results regarding the tissue distribution of QD. The results indicated that (a) intradermally injected nanoscale QD remained as a deposit in skin and penetrated the surrounding viable subcutis, (b) QD were distributed to draining lymph nodes through the subcutaneous lymphatics and to the liver and other organs, and (c) sentinel organs are effective locations for monitoring transdermal penetration of nanoscale materials into animals.

Keywords

nanoparticles; nanoscale materials; quantum dots; sentinel organs; biodistribution

[*]To whom correspondence should be addressed: Division of Biochemical Toxicology, HFT-110, National Toxicology Program Center for Phototoxicology, National Center for Toxicological Research, U.S. Food & Drug Administration, 3900 NCTR Rd, HFT-110, Jefferson, Arkansas 72079, Tel: (870)543-7672, or -7137, FAX: (870)543-7136, Paul.Howard@fda.hhs.gov.

INTRODUCTION

Nanotechnology is the manipulation or synthesis of materials at the atomic level that have at least one dimension between approximately 1 to 100 nm (Murray *et al.*, 2000; Oberdorster *et al.*, 2005; NNI, 2006). The nanometer size of some of these materials results in unique and tunable properties can be exploited, and has led to nanotechnology being hailed as the "next technological revolution". Industry and governments worldwide have invested considerable resources into the research and development of nanotechnology-based products that is expected to reach $28 billion by 2008 (Kamalick, 2004). While the investment during this early period of growth has focused on product development, little information regarding the adverse effects of engineered nanometer sized materials on biologic systems has been published. Many agree that there needs to be a balance of investment in nanotechnology development and understanding toxicity of the products (Hardman, 2006; Davies, 2006; Maynard, 2006).

Nanoscale titanium dioxide and zinc oxide, below approximately 200 nm diameter, do not reflect visible light yet still reflect or absorb ultraviolet light. In particular, their ability to interact with UVA light is unique as compared to many organic sunblock agents and for this reason they are included as physical sunblocks to increase the sun protection factor (SPF) in topically applied cosmetics and sunscreens (Innes *et al.*, 2002; Popov *et al.*, 2005, 2006). Titanium dioxide can exist in several physical forms (anatase, rutile, amorphous, and brookite; see for example Mogyorósi *et al.*, 2003). Irradiation of the anatase form of titanium dioxide with light below 380 nm results in the generation of reactive oxygen species (Hoffman *et al.*, 1995; Blake *et al.*, 1999; Mills and LeHunte, 1997) resulting in photocatalytic killing of bacteria (Gaswami *et al.*, 1997; Stevenson *et al.*, 1997; Sunada *et al.*, 1998; Jacoby *et al.*, 1998; Byrne *et al.*, 1998; Maness *et al.*, 1999), photodecomposition of dyes (Aleboyeh *et al.*, 2003, and Neamtu *et al.*, 2004, Moraes *et al.*, 2004, Wahi *et al* 2005, 2006), and use as a photocatalyst in dye-sensitized solar cells (Kusama and Arakawa, 2003). This generation of reaction oxygen species can be prevented by physically separating the titanium dioxide crystal from oxygen or water with an inert coating (*i.e.* insulator or coating) such as zirconium, alumina, or silica (Mills and LeHunte, 1997).

Whether nanoscale particles can penetrate into skin has been of increasing interest to toxicologists and nanotechnologists alike; the existing reports illustrate that this is a complex question whose answer may depend on particle size, surface coating, medium as well as skin model. Specific to the problem of nanoscale titanium dioxide into skin, investigators have found in some cases evidence for penetration as well as evidence to the contrary (Tan *et al.*, 1996; Landsdown and Taylor, 1997; Pflücker *et al.*, 2001; Lademann *et al.*, 1999; Bennat and Müller-Goymann, 2000; Schulz *et al.*, 2002; Menzel *et al.*, 2004). The most recent studies of Gamer et al. (2006) and Mavon et al. (2007) find that titanium dioxide in an oil and water emulsion does not penetrate either porcine or human skin *in vitro*, respectively. However, other nanoscale materials such as quantum dots and tethered-fullerenes have been observed to penetrate skin *in vitro* (Ryman-Rasmussen *et al.*, 2006, Rouse *et al.*, 2007). If there are circumstances under which nanoscale titanium dioxide does penetrate and reside in the skin, then there is potential for biological effect. The material can serve as a catalyst for continued generation of reactive oxygen species upon irradiation with UV containing light (*e.g.* sunlight), resulting in damage to the skin (*e.g.* photoaging or carcinogenesis). The possibility of this unwanted toxicity will depend on the ability of the nanoscale particle to penetrate the skin, and the photoactivity of the nanoscale particle, neither of which is fully characterized at this time for nanoscale materials included in topically applied cosmetics and sunscreens.

In an effort to understand the biodistribution of nanoscale materials intradermally injected into skin we have chosen to use poly(ethylene glycol) (PEG) coated quantum dots (QD) as surrogates for uncharged, biologically inert nanoscale materials. QD (semiconductor nanocrystals) are fluorescent semiconductor inorganic nanocrystals that have unique optical and physiochemical properties (Nirmal *et al.*, 1996; Knight *et al.*, 2004; Gao *et al.*, 2005; Hardman, 2006). QDs offer strong fluorescence at narrow and tunable wavelengths across the visible and infrared wavelengths, and can be excited with light over a broad range of energies. In addition, their high quantum yields, substantial Stoke's shifts, and photostability make them of great interest as imaging agents in biological systems (Alivisatos *et al.,* 2005; Azzazy *et al.*, 2006; Leary *et al.*, 2006; Pinaud *et al.*, 2006; Smith *et al.*, 2006).

We have taken advantage of the relative ease of imaging of QD and used them as surrogates for similar sized nanoscale materials such as titanium dioxide. In addition, because cadmium is not an essential element and occurs at low concentrations in tissues, we have used inductive-coupled plasma mass spectrometry (ICP-MS) to monitor cadmium levels as an indication of the presence of QD in tissues.

MATERIALS AND METHODS

Materials

Preparation of quantum dots—Different colors of quantum dots (QDs) with core/shell structures were synthesized according to published methods except minor modifications to the shell growth temperature (CdSe as the core; Yu *et al.,* 2003). For this work, we used 180°C to grow a CdS shell to facilitate a red color emission. The QDs were purified and stored in chloroform before further treatment. QD concentrations were determined using the extinction coefficients and the error in these measurements was estimated by comparing the wide range of reported extinction coefficients in the literature (Yu *et al.*, 2004a).

Preparation of water-soluble quantum dots—Highly uniform quantum dots can only be synthesized in organic solutions, thus biological studies require that the materials be encapsulated in order to form stable solutions in aqueous buffers. PEG containing amphiphilic co-polymers were used for this purpose. The coating material is first prepared through the reaction of a commercial poly(maleic anhydride-alt-1-octadecene) (PMAO, M_n = 30000–50000, Aldrich Chem. Co., Milwaukee, WI) polymer and an amino terminated PEG methyl ether (mPEG-NH_2, MW 6000, 9900 and 19300; Nektar, CA)with typical molar ratios of 1:50 (PMAO:PEG).

The monodispersed QDs (purified and dispersed in chloroform) and the amphiphilic polymer (PMAO-PEG) were mixed in chloroform and stirred overnight (room temperature) (molar ratio of QD:PMAO-PEG ranged from 1:5 to 1:30). Purified water was then added to the chloroform solution of the complexes with a 1:1 volume ratio; chloroform was gradually removed by rotary evaporation at room temperature, and resulted in clear and colored solution of water-soluble QDs. This transfer process had a 100% efficiency and no precipitate was observed; however, to remove possible larger contaminants, the solutions were passed through a 0.2-micrometer Nylon syringe filter. The nanoscale QD were concentrated using ultracentrifugation (typically 200,000 – 300,000 *g* for 2 hours; Beckman Coulter Optima L-80XP; Beckman Coulter, Inc., Fullerton, CA) with the soluble excess amphiphilic polymer being decanted. Further details of this procedure and subsequent characterization of these materials are described in the work of Yu *et al* (2007).

Quantum dot characterization—Absorption spectra of QDs were measured by a Varian Cary 5000 UV-VIS-NIR spectrophotometer (Varian Inc., Palo Alto, CA).

Photoluminescence (PL) spectra (for QDs) were recorded on a Jobin Yvon Spex Fluorolog 3 fluorescence spectrophotometer (Horiba Jobin Yvon Inc., Edison, NJ).

Transmission electron microscopy (TEM) specimens were made by evaporating one drop of nanocrystal solutions on carbon coated copper grids. The TEM micrographs were taken by Jeol FasTEM 2010 transmission electron microscope (Tokyo, Japan). The size and size distribution data were obtained by counting >1000 individual particles using Image-Pro Plus 5.0 (Media Cybernetics Inc., Silver Spring, MD) (Yu *et al.,* 2004a, 2004b).

Size exclusion chromatography (SEC) was applied to measure the hydrodynamic diameters of the water-soluble QDs on an Agilent high-performance liquid chromatograph (1100 series; Agilent Technologies Inc., Santa Clara, CA) equipped with hydroxylated polymethacrylate-based gel (Ultrahydrogel 1000 and 2000, Waters Corp., Milford, MA) columns (Al-Somali *et al.*, 2004; Krueger *et al.*, 2005). Dynamic light scattering (DLS) was also employed to measure the hydrodynamic diameters of the water-soluble QDs using a Brookhaven 90Plus particle analyzer (Brookhaven Instr. Corp., Holtsville, NY) at 25°C.

Animals—Isolator reared, *Helicobacter*-free female Crl: SKH-1 (hr^{-}/hr^{-}) hairless mice were obtained from Charles River (Portage, MI) at 5 weeks of age. The mice were housed for two-weeks in the NCTR Quarantine Facility and acclimated for an additional week prior to use. The treatment of the mice conformed to the institutional Animal Care and Use Committee guidelines at this American Association for Laboratory Animal Science (AALAS) accredited facility.

Treatment of mice—At 9 weeks of age, mice were weighed and anesthetized intraperitoneally with sodium pentobarbital (25 mg/kg body weight). Anesthetized mice were injected intradermally (ID) in the right dorsal flank with either 5 μl of 9.5 μM QD (48 pmoles) or sterile saline using a Hamilton gas-tight syringe (Hamilton Company, Reno, NV) equipped with a 3/8-inch, 26 gauge needle with a 30° (intradermal) bevel. The syringe containing QD was visualized with a hand-held UVA light (UVP UVGL-58; UVP Inc., San Gabriel, CA) to confirm correct loading of the syringe and the absence of bubbles in the syringe. Proper ID injection was confirmed by the formation of a small induration at the site of injection. Dissection of the site of practice injections and fluorescent macrophotography revealed that injection material did not penetrate to the subcutaneous tissue (data not shown). Immediately following ID injection, the site of application was imaged under UVA illumination and photographed using a Canon EOS D60 camera equipped with a Canon 100 mm EF Macro lens (Canon Corporation USA, Inc.). Images were recorded as 6 megapixel images in the raw-file format.

At 0, 4, 8, 12 and 24 hr following ID dosing, the mice (n=4 time point) were euthanized using gaseous carbon dioxide and again imaged under UVA illumination. The following tissues were removed and stored at −20 °C prior to elemental analysis: blood (obtained by cardiac puncture); skin (site of injection and control site); axillary, brachial, and inguinal lymph nodes; liver; hepatic lymph node; kidneys; spleen; stomach; intestine; cecum contents; uterus; bladder; brain; femur. Tissues from one mouse that was sacrificed 24 hrs after QD injection were placed in 10% neutral buffered formalin, and after 48 hours dehydrated with ethanol, embedded in paraffin blocks, and sectioned at 4 microns. The tissue sections were mounted onto slides and were not stained or covered.

ICP-MS quantification of cadmium and selenium—Inductively coupled plasma mass spectrometry (ICP-MS) was performed utilizing a Fisons PlasmaQuad 3 quadrupole instrument (Thermo Electron Corp., Franklin, MA). Samples that were in excess of the suitable weight for analysis were minced, water added (18 MΩ, Barnstead, Dubuque, IA),

and homogenized 3 time for 30 sec at 24,000 rpm using am Ultra-Turraz T25 homogenizer (IKA, Staufen, Germany). Fractions of the homogenates, blood (0.1 mL), or tissues (0.2 g), and 1 mL of 2% HNO_3 (Ultrex, J.T. Baker, Phillipsburg, NJ) and 1 mL 70% HNO_3 (Ultrex) were combined in a microwave digestion vessel (Xpress PTFA, 55 mL) and digested at 300 Watts, 200°C, and 220 psi using a microwave accelerated reaction system (MARS, CEM, Matthews, NC) for 35 min. Recovery was accomplished by adding Cd and Se standards (SPEX CertiPrep Claritas, Metuchen, NJ) at 10 ng/mL in 1 mL 2% HNO_3 (Ultrex) prior to homogenization. The ICP-MS instrument was initialized, optimized, and standardized using the manufacturers recommendations. Tuning of the ion lenses was accomplished using a standard containing 1 ng/mL ^{9}Be, ^{115}In, and ^{238}U in addition to other elements. When optimized the ion count rate for ^{115}In was approximately 25,000 cps/ppb. Standardization was performed using 1–100 ng/mL multi-element standards. Quantification was accomplished using ^{112}Cd, ^{114}Cd, and ^{82}Se isotopes. The limits of detection (3 σ) averaged 3 pg/mL for Cd and 70 pg/mL for Se. The limits of quantification (10 σ) were 10 pg/mL for Cd and 200 pg/mL for Se.

Recovery from control tissue samples spiked with Cd and Se standards averaged 72.4% for Cd and 80.1% for Se.

Fluorescence Microscopy—Photomicrographs were taken using a Leica DM RA2 photomicroscope (Leica Microsystems GmbH, Wetzlar, Germany) equipped with a 100 W halogen light source and SPOT RT-SE slider high resolution CCD camera/digital imaging system (Diagnostic Instruments, Sterling Heights, MI). Images of the tissues with bright field illumination were obtained to show structure. In the fluorescence mode, a filter set consisting of a 415WB/100 excitation filter, a 475DCLP dichroic filter, and 620WB20 emission filter (Omega Optical Inc., Brattleboro, VT) were used to selectively visualize the 621 nm emission from the QD. Images were captured at 20× and saved as 16 bits per pixel SPOT files. The images were then imported into SPOT proprietary software and converted to 12 bit per pixel jpeg files for image export.

Chemicals—Nembutal (sodium pentobarbital solution) (50 mg/mL) was obtained from Abbott Laboratories (North Chicago, IL) and diluted to 6.5 mg/mL using 0.9% sterile injectable sodium chloride solution (Abbott Laboratories) prior to use. All other reagents were the best analytical grade available.

Statistical Analysis

The cadmium levels at each time point were analyzed using a one way analysis of variance with comparison to the control (0 hr) and all groups using Holm-Sidak method. Analyses were performed using SigmaStat (Jandel Scientific Corp., San Rafael, CA) and comparisons were considered significant when the probability value was less than 5% ($p<0.05$).

RESULTS

Characterization of QD

The QD synthesized for this study yielded a fluorescence emission of 621 nm when irradiated with light of wavelength <610 nm. The structure of the QD was evaluated using high resolution TEM (Figure 1). The CdSe core with CdS shell had a nail shape with a head width of 5.8 ± 0.97 nm and length of 8.4 ± 1.9 nm.

The amphiphilic polymer itself contributes a large fraction to the overall hydrodynamic diameter. Dynamic light scattering (DLS) is a semi-quantitative method for hydrodynamic diameter measurement of highly absorptive materials below 50 nm; this method indicated

these materials in a wide range of buffers and water were 39 ± 4 nm in diameter. A more accurate method for particle size measurement in solution is size exclusion chromatography (SEC) (Al-Somali *et al.,* 2004; Kreuger *et al.,* 2005); in this method particle size is found from the retention times, and this is converted to hydrodynamic diameter from a calibration generated by running known standards through the SEC system. In pure water, these water soluble were found to have hydrodynamic diameters of 37 ± 1 nm.

Concentration of quantum dot solutions

The water-soluble QD's concentration is determined by measuring its absorbance spectrum and then calculated from Lambert-Beer law, $A = \varepsilon\, b\, C$, where A is the optical density, ε is the extinction coefficient of the core/shell QD, b is the light path length, and C is the core/shell QD concentration. Extinction coefficients for plain core QD are available from literature (Yu *et al*., 2004a), but these data are not applicable to complex structures like core/shell QDs due to their complicated structure (including shell thickness) and chemical composition. For our CdSe/CdS core/shell QD, we first obtained the initial quantity (mole number or particle number calculated from published ε data; Yu *et al*., 2004a) of plain core CdSe QD in the synthesis flask and assumed the same quantity of core/shell particles produced. We determined the extinction coefficient of this core/shell QD as 170,000 ± 22,500 M cm^{-1} and determined a final concentration of 19 ± 2.5 μM. ICP-MS analysis of the QD solution demonstrated 43 μg/mL of Cd (38 mM) and 4.7 μg/mL of Se (6 mM) for a Cd:Se ratio of 6.4:1.

Fluorescence of intradermally injected QD

The female SKH-1 hairless mice were injected on the right dorsal flank with 5 μL of 9.5 μM QD solution. Immediately following intradermal injection, red fluorescent QD could be seen during ultraviolet-A illumination migrating in the skin lymphatics towards the direction of the regional draining lymph nodes (Figure 2A and 2B). This visual phenomenon decreased with time and was not apparent by 6 hours post-injection. At sacrifice, the skin and regional draining lymph nodes were very fluorescent under ultraviolet-A illumination (not shown).

Disposition of cadmium in tissues

Mice (n=4 time point) were sacrificed immediately or 4, 8, 12, and 24 hours following intradermal injection of 5 μL of QD in the right dorsal flank. The average total cadmium detected in sham injected mice was 199 ± 14 ng (mean ± SE, n=6) with the following distribution: skin, 0.63 ± 0.23 ng; lymph nodes, 0.46 ± 0.07 ng; liver, 20.0 ± 1.8 ng; kidney, 20.9 ± 1.5 ng; blood, 11.7 ± 2.9 ng; cecum contents, 127.7 ± 12.5 ng. The average total cadmium recovered from mice injected with QD at 0 hr was 24.57 ± 1.72 μg (mean ± SE, n=4). Because a 5 μL injection of QD should contain 21.5 μg cadmium and 2.35 μg selenium, the average intradermal dose was 114.3 ± 8.0% of the target dose.

The amount of cadmium that was recovered from the site of injection and all tissues analyzed for the presence of cadmium was 100.0 ± 4.9% at 0 hr, and averaged 64.9 ± 6.0% at subsequent time points. The remaining QD (that is cadmium) present in the skin of the mice at the site of injection is shown in Figure 3. There was an initial and sustained loss of approximately 40% of the cadmium from the site of injection, where the value at all time-points was significantly reduced from that of the 0 hour value. The apparent decrease at 8 hours and rise in cadmium levels at 12 hours is not statistically significant and could be the result of small numbers of animals and variability or variability in quantity of QD injected; however, the values at 4, 12, and 24 hours are essentially equal at approximately 60% of injected cadmium remaining at site of injection.

The results of the analysis of various organs for cadmium content are shown in Figure 4 (n=4 mice/time point). There was no detectible cadmium in the liver of the mice at 0 hr. The cadmium level increased at 13 and 24 hours to average totals of 1.432 ± 0.554 μg and 1.572 ± 0.353 μg, respectively (mean ± SE). These values are significantly different than the value at 0 hr, and correspond to 5.83% and 6.40% of the administered dose of QD as cadmium.

Lymph nodes taken from mice at 0 hr contained 2.7 ± 3.7 ng of cadmium, which increased to 297 ± 174 ng and 262 ±55 ng at 12 hrs and 24 hrs, respectively (mean ± SE). The levels of cadmium at 12 hrs and 24 hrs were significantly increased over the levels at 0 hr, and corresponded to 1.21% and 1.07% of the initial dose of cadmium in the QD (Figure 4).

Accumulation of cadmium in the kidneys is also presented in Figure 4. The level of cadmium at 0 hr (0 ng) significantly increased to 63 ± 13 ng at 12 hrs and 126 ± 19 ng at 24 hrs (mean ± SE). These values represented 0.26% and 0.51% of the administered dose, respectively.

Significant increases in cadmium were detected in several other tissues (Figure 5) including the spleen, hepatic lymph node, and heart. In the spleen, cadmium levels increased from 0.1 ng total cadmium to significantly elevated levels of 40 ± 22 ng (0.16% ± 0.09% of dose) and 44 ± 20 ng (0.18% ± 0.08% of dose) at 12 hrs and 24 hrs, respectively (mean ± SE). In the hepatic lymph node, the cadmium level at 0 hr was 0.1 ng, increasing to 3 ± 1.9 ng (0.012% ± 0.005% of dose) and 5.4 ± 4.6 ng (0.022% ± 0.013% of dose) at 12 hrs and 24 hrs, respectively (mean ± SE).

The final tissue where significant increases in cadmium levels were detected was the heart (Figure 5) increasing from 0.1 ng at 0 hr to 3.4 ± 0.8 ng and 3.8 ± 0.5 ng at 12 hrs and 24 hrs, respectively (mean ± SE); however, the animals were terminated using cardiac puncture and exanguination. The levels of cadmium in the blood did not change during the 24 hrs of the study, and was 32.4 ± 3.1 ng cadmium/mL blood. As a result, contamination of the heart with as little as 100 μL of blood could be responsible for the cadmium that was detected.

No significant trends were detected in the cadmium levels detected in the brain, lung, urinary bladder, femur, or cecum contents in the mice (data not presented).

Fluorescence microscopy of QD in tissues

The presence of fluorescent QD at the site of injection and in the regional draining lymph nodes were confirmed using fluorescence microscopy as shown in Figure 2C–2H. Mice were sacrificed 24 hours following intradermal injection and the skin at the site of injection, skin from a non-injection site, and lymph nodes (axillary, brachial, inguinal) were removed, fixed in 10% neutral buffered formalin, and sectioned for microscopy. After 24 hrs, the remaining highly red fluorescent QD at the site of injection are clearly visible at the site of injection, and had dispersed throughout the dermis but not the epidermis (Figure 2C–D). Red fluorescence was not detected in skin from the same mouse taken from a site distant from the QD injection (images not shown). Since the QD were injected on the right dorsal side of the mouse, fluorescent QD were detected in the right axillary (Figure 2E–F) and right brachial (Figure 2G–H) but not left axillary or brachial lymph nodes lymph nodes (images not shown). The red fluorescent QD in the right axillary lymph nodes were predominantly in the supcapsular and trabecular sinuses.

DISCUSSION

We have demonstrated that intradermally injected QD remained as a depot in skin, penetrated the surrounding viable subcutis, and were visibly distributed to regional draining

lymph nodes and other organs apparently through the subcutaneous lymphatics. Approximately 6%, 1% and 0.5% of the administered cadmium from the QD accumulated in the liver, regional draining lymph nodes, and kidneys, respectively, at 24 hrs after the intradermal injection. Using fluorescence microscopy, the QD were visible in the skin and regional draining lymph nodes. Therefore, if these QD penetrate the epidermis into the dermis following topical application, based on the results in this paper we would expect approximately 7.5% of the dose to accumulate in the liver, lymph nodes and kidneys during the first 24 hours. These data do not necessarily predict what could happen with other nanoparticles. There could be obvious differences in the kinetics of the transport and distribution of nanoparticles based on size and chemical nature of the outer coating of the nanoparticle; however, these current results demonstrate the potential of using ICP-MS analysis of sentinel organs as dosimeters of nanoscale material penetration into the dermis and migration within the body.

The QD used in this paper were PEG coated with a mean diameter of 37 nm. Although few *in vivo* studies exist, they suggest that QD may be systemically distributed in murine and porcine animal models and accumulate in a variety of organs and tissues similar to our findings. Intradermal injection into the paw of a mouse with near infrared (NIR) emitting QD with a hydrodynamic diameter of 15–20 nm resulted in QD entering the lymphatics and migrating within minutes to an axillary location (Kim *et al.*, 2004). Additionally, when NIR emitting QD were injected intradermally on the thigh of a pig, a surgeon was able to follow lymphatic flow from lymph channels that diverge from the injection site and then coalesce into the sentinel lymph node within 3–4 min, and where approximately 2–4% of the injected QD accumulated in the sentinel lymph node based on fluorescence measurements (Kim *et al.*, 2004). This level of migration to the lymph is remarkably similar to our results where the maximum level of QD in the lymph nodes was 1.2% of the injected dose (Figure 4).

Fluorescence microscopy of the regional draining lymph nodes from QD injected animals exhibited fluorescence that was mainly localized in subcapsular and trabecular lymphatic sinuses. In agreement with our findings, analysis of resected tissue in the study of Kim *et al.* (2004) showed that NIR emitting QD were confined to the outermost rim of the lymph node. These data are consistent with the known sieving properties of the lymph node's subcapsular sinus. Uren *et al.* (2004) and Kim *et al.* (2004) have suggested there is a critical hydrodynamic diameter range of 5–50 nm needed for retention of QD in the sentinel lymph node.

The administration of QD injected by other routes results in a different disposition *in vivo*. The intravenous injection of QD-labeled EL-4 mouse lymphoma cells into mice resulted in the elimination of approximately 70% of the QD-labeled cells within 2 hrs (Hoshino *et al.*, 2004). QD-label accumulation 7 days later was greatest in the spleen and lungs, followed by lesser accumulation in the kidneys and liver based on fluorescence measurements (Hoshino *et al.*, 2004). The accumulation of the QD-labeled cells in the spleen is consistent with the biology of T-lymphocyte accumulation and processing in the spleen (Hoshino *et al.*, 2004). In a separate study, QD labeled cells were injected into the tail veins of C57BL/6 mice where QD were observed to accumulate in the lungs, liver and spleen, with rapid clearance from the circulation (Voura *et al.*, 2004).

In a study by Ballou *et al.* (2004) QD that had different coatings including methoxy-terminated PEG (molecular weight of 750 Da; mPEG-750), carboxy-terminated PEG (molecular weight of 3,400 Da; COOH-PEG-3400), and ethoxy-terminated PEG (molecualar weight of 5,000 Da; mPEG-5000) were used in an *in vivo* study. Immediately following intravenous injection in mice, fluorescence was noted in the superficial vasculature and QD fluorescence was apparent in the liver, skin, and bone marrow. The

fluorescence in the skin was initially punctuate, then spread across the skin, and was not present after 24 hrs. The methoxy-terminated mPEG-750 QD and carboxylic acid-terminated COOH-PEG-3400 QD were cleared from circulation by 1 hr after intravenous injection (half-life <12 min), whereas the ethoxy-terminated mPEG-5000 QD remained in circulation for at least 3 hr (half-life 50–140 min). The longer serum half-life of the ethoxy terminated QD may be due to lack of reticuloendothelial uptake or decreased clearance by renal filtration (Gao *et al.*, 2005). The methoxy-terminated mPEG-750 QD were observed in the lymph nodes, liver, and bone marrow after 24 hours, with significantly less retention of the carboxylic acid-terminated COOH-PEG-3400 and ethoxy-terminated mPEG-5000 QD in the same tissues. was observed in lymphatic tissue compared with bone marrow, liver, and spleen. The presence of QD in the intestinal contents suggested excretion of QD from the liver (Ballou *et al.*, 2004).

These and other *in vivo* studies suggest that, regardless of the QD coating, vertebrate systems tend to recognize QD as foreign, with elimination of the materials through the primary excretory organ systems including the liver, spleen, and lymphatic systems (Hardman, 2006); however, this a rough generalization, and discrepancies in the literature exist. For instance, subcutaneous injection of PEG coated CdSe/ZnS QD in mice showed clearance of the QD from the site of injection, with accumulation of QDs in lymph nodes similar to the studies we are reporting in this paper (Hardman, 2006). Peptide-coated QD were first used to target tissue-specific vascular markers by intravenous injection in mice (Akerman *et al.*, 2002), where it was observed that modification of lung- and tumor-targeting peptide-conjugated CdSe/ZnS QD with a PEG coating nearly eliminated nonspecific elimination of QD via the lymphatic system. Their studies provide evidence that QD outer coating will dictate systemic distribution independent of the core QD properties (Hardman, 2006). QD which are not PEGylated, and that lack specialized functional groups for cell targeting, have been shown to be incorporated via endocytic mechanisms by a variety of cell types, both *in vivo* and *in vitro* (Hardman, 2006, Chang et al 2006). Several studies have shown nonspecific QDs to adhere to cell surfaces, possibly through interactions of QD with glycoproteins and glycoplipids in cell membranes (Hardman, 2006). Although many studies indicate endocytic processes and intracellular vesicular trafficking and storage of QDs, the exact mechanisms remain to be elucidated. In contrast, QDs bearing natural ligands specific for cell receptors and cell membrane proteins have been shown to be specific for given cell membrane proteins/receptor types (Hardman, 2006).

In order to determine the long-term stability and tissue deposition of QD *in vivo*, a Balb/C mice were intravenously injected with methoxy-terminated mPEG-750 QD and imaged during necropsy at 15 min, 1 day, 3 days, 7 days, 28 days, and 133 days later (Ballou *et al.*, 2004). The QD remained in the liver, lymph nodes, and bone marrow for at least one month with fluorescence decreasing over time. By 133 days postinjection, the QD fluorescence was visible by fluorescence microscopy in the lymph nodes, liver, spleen, and bone marrow. As part of this study, transmission electron microscope images of a mouse spleen cell 24 h postinjection showed localization of the QD in endosomes. These results suggest that the QD detected in the liver and lymph nodes in our study at 24 hrs, would possibly have remained in those tissues for many weeks.

Fischer *et al.* (2006) studied the pharmacokinetics of mercaptoundecanoic acid coated (QD-LM) and bovine serum albumin coated (QD-BSA) quantum dots in rats following intravenous injections using ICP atomic emission spectroscopy (ICP-AES) to detect the cadmium in blood and tissues. The mean hydrodynamic radius of the QD-LM was 25 nm and the QD-BSA was 80 nm in diameter. The authors showed that the quantum dots were cleared quickly from the blood with half-life's of 59 min for QD-LM and 39 min for QD-BSA following intravenous injections. Ninety minutes after injection, 36% of the QD-LM

and 99.5% of the QD-BSA were contained in the liver. Quantum dots were detected at much lower levels in the spleen (~2% of dose) and were not detected in the lymph nodes using ICP-MS, but were visible in the lymph nodes and bone marrow using fluorescence microscopy. Our work is in agreement with the studies reported by Fischer *et al.* (2006) where the liver is the primary organ of nanoparticle deposition, this in spite of the fact that our quantum dots were PEG coated while those used in Fischer *et al.* (2006) were coated with an organic acid and bovine serum albumin. This observation also supports our use of the liver as a sentinel organ in future studies with nanoparticles.

In summary, we have demonstrated that regional lymph nodes, liver, kidney and spleen are sentinel organs for the detection of intradermally administered QD that are PEG coated and are approximately 37 nm in diameter. These results are consistent with the studies described above using QD coated with PEG and other coatings. The difference in our studies was the QD were detected based on the cadmium content of the quantum core using ICP-MS, and the presence of QD was confirmed using fluorescence microscopy. It is our conclusion that regional lymph nodes and liver can be used as sentinel organs to determine the penetration through the skin by QD and possibly other nanoparticles.

Acknowledgments

The authors would like to thank Drs. Frederick Beland, John Bucher, Dori Germolec, Sally Tinkle, and William Tolleson for critical review of the manuscript. This research was supported by an Interagency Agreement (IAG 224-93-0001) between the U.S. Food & Drug Administration and the Intramural Research Program of the National Institutes of Health (NIH), National Institute of Environmental Health Sciences. The contents of this manuscript do not necessarily reflect the views and policies of the U.S. Food & Drug Administration or the National Institute of Environmental Health Sciences. The mention of trade names or commercial products does not constitute endorsement or recommendation for use.

References

Akerman ME, Chan WC, Laakkonen P, Bhatia SN, Ruoslahti E. Nanocrystal targeting in vivo. Proc Natl Acad Sci U S A. 2002; 99:12617–12621. [PubMed: 12235356]

Aleboyeh A, Aleboyeh H, Moussa Y. “Critical” effect of hydrogen peroxide in photochemical oxidative decolorization of dyes: Acid Orange 8, Acid Blue 74 and Methyl Orange. Dyes and Pigments. 2003; 57:67–75.

Alivisatos AP, Gu W, Larabell C. Quantum dots as cellular probes. Annu Rev Biomed Eng. 2005; 7:55–76. [PubMed: 16004566]

Al-Somali AM, Kreuger KM, Falkner JC, Colvin VL. Recycling size exclusion chromatography for the analysis and separation of nanocrystalline gold. Analy Chem. 2004; 76:5903–5910.

Azzazy HME, Mansour MMH, Kazmierczak SC. Nanodiagnostics: A new frontier in clinical laboratory medicine. Clin Chem. 2006; 52:1238–1246. [PubMed: 16709623]

Ballou B, Lagerholm BC, Ernst LA, Bruchez MP, Waggoner AS. Noninvasive imaging of quantum dots in mice. Bioconjug Chem. 2004; 15:79–86. [PubMed: 14733586]

Bennat C, Müller-Goymann CC. Skin penetration and stabilization of formulations containing microfine titanium dioxide as physical UV filter. Int J Cosmetic Sci. 2000; 22:271–283.

Blake DM, Maness PC, Huang Z, Wolfrum EJ, Jacoby WA, Huang J. Application of the photocatalytic chemistry of titanium dioxide to disinfection and the killing of cancer cells. Sep Purif Methods. 1999; 28:1–50.

Byrne JA, Eggins BR, Brown NMD, McKinnery B, Rouse M. Immobilisation of TiO_2 powder for the treatment of polluted water. Appl Catal B Environ. 1998; 17:25–36.

Chang E, Thekkek N, Yu WW, Colvin VL, Drezek R. Evaluation of Quantum Dot Cytotoxicity Based on Intracellular Uptake. Small. 2006; 2(12):1412–1417. [PubMed: 17192996]

Davies, JC. Project on Emerging Nanotechnologies: Managing the effects of nanotechnology. Woodrow Wilson International Center for Scholars; 2006. (Available at http://www.wilsoncenter.org/index.cfm?topic_id=166192&fuseaction=topics.item&news_id=165552)

Fischer HC, Liu L, Pang KS, Chan WCW. Pharmacokinetics of nanoscale quantum dots: *In vivo* distribution, sequestration, and clearance in the rat. Adv Funct Mater. 2006; 16:1299–1305.

Gao X, Yang L, Petros JA, Marshall FF, Simons JW, Nie S. *In vivo* molecular and cellular imaging with quantum dots. Curr Opin Biotechnol. 2005; 16:63–72. [PubMed: 15722017]

Gaswami DY, Trivedi DM, Block SS. Photocatalytic disinfection of indoor air. J Sol Energy Eng. 1997; 119:92–96.

Hardman R. A toxicologic review of quantum dots: toxicity depends on physicochemical and environmental factors. Environ Health Perspect. 2006; 114:165–172. [PubMed: 16451849]

Hoffman MR, Martin ST, Choi W, Bahnemann DW. Environmental applications of semiconductor photocatalysis. Chem Rev. 1995; 95:69–96.

Hoshino A, Hanaki K, Suzuki K, Yamamoto K. Applications of T-lymphoma labeled with fluorescent quantum dots to cell tracing markers in mouse body. Biochem Biophys Res Commun. 2004; 314:46–53. [PubMed: 14715244]

Innes B, Tsuzuki T, Dawkins H, Dunlop J, Trotter G, Nearn MR, McCormick PG. Nanotechnology and the cosmetic chemist. Cosmet, Aerosols Toilet Austr. 2002; 15:10–12. 21–24.

Jacoby WA, Maness P-C, Wolfrum EJ, Blake DM, Fennel JA. Mineralization of bacterial cell mass on a photocatalytic surface in air. Environ Sci Technol. 1998; 32:2650–2653.

Kamalick, J. Analysis: Nanomaterials to see huge growth over 5 years. Chemical News and Intelligence. 2004 Feb 5. (Available at http://www.chemweb.com/alchem/articles/1075467726478.html)

Kim S, Lim YT, Soltesz EG, De Grand AM, Lee J, Nakayama A, Parker JA, Mihaljevic T, Laurence RG, Dor DM, Cohn LH, Bawendi MG, Frangioni JV. Near-infrared fluorescent type II quantum dots for sentinel lymph node mapping. Nature Biotechnology. 2004; 22:93–97.

Knight, A.; Gaunt, J.; Davidson, T.; Chechik, V.; Windsor, S. Evaluation of the suitability of quantum dots as fluorescence standards. NPL Report DQL-AS 007. 2004. (Available at http://www.mfbprog.org.uk/themes/theme_publications_item.asp?intThemeID=10&intPublicationID=968)

Kreuger KM, Al-Somali AM, Falkner JC, Colvin VL. Characterization of nanocrystalline CdSe by size exclusion chromatography. Analy Chem. 2005; 77:3511–3515.

Kusama H, Arakawa H. Influence of pyrimidine additives in electrolytic solution on dye-sensitized solar cell performance. J Photochem Photobiol A: Chem. 2003; 160:171–179.

Lademann J, Weigmann HJ, Rickmeyer C, Barthlemes H, Schaefer H, Mueller G, Sterry W. Penetration of titanium dioxide miroparticles in a sunscreen formulation into the horny layer and the follicular orifice. Skin Pharmacol Appl Skin Physiology. 1999; 12:247–256.

Lansdown ABG, Taylor A. Zinc and titanium oxides: promising UV-absorbers but what influence do they have on the intact skin? Int J Cosmetic Sci. 1997; 19:167–172.

Leary SP, Liu CY, Apuzzo MLJ. Toward the emergence of nanoneurosurgery: Part II – Nanomedicine: Diagnostics and imaging at the nanoscale level. Neurosurgery. 2006; 58:805–823. [PubMed: 16639314]

Maness P-C, Smolinski S, Blake DM, Huang Z, Wolfrum EJ, Jacoby WA. Bactericidal activity of photocatalytic TiO_2 reaction: toward an understanding of it killing mechanism. Applied Environ Microbiol. 1999; 65:4094–4098.

Maynard, AD. Project on Emerging Nanotechnologies: Nanotechnology, A Research Strategy for Addressing Risk. Woodrow Wilson International Center for Scholars; 2006. (Available at http://www.wilsoncenter.org/index.cfm?topic_id=166192&fuseaction=topics.event_summary&event_id=194810)

Menzel F, Reinert T, Vogt J, Butz T. Investigations of percutaneous uptake of ultrafine TiO_2 particles at the high energy ion nanoprobe LIPSION. Nuclear Instruments and Methods in Physics Research B. 2004:219–229. 82–86.

Mills A, Le Hunte S. An overview of semiconductor photocatalysis. J Photochem Photobiol A Chem. 1997; 108:1–35.

Mogyorósi K, Dékány I, Fendler JH. Preparation and characterization of clay mineral intercalated titanium dioxide nanoparticles. Langmuir. 2003; 19:2938–2946.

Moraes JEF, Quina FH, Nascimento CAO, Silva DN, Chiavone-Filho O. Treatment of saline wastewater contaminated with hydrocarbons by the photo-Fenton process. Environ Sci Technol. 2004; 38:1183–1187. [PubMed: 14998035]

Murray CB, Kagan CR, Bawendi MG. Synthesis and characterization of monodisperse nanocrystals and close-packed nanocrystal assemblies. Ann Rev Mater Sci. 2000; 30:545–610.

NNI (National Nanotechnology Initiative). http://www.nano.gov

Neamtu M, Yediler A, Siminiceanu I, Macoveanu M, Kettrup A. Decolorization of disperse red 354 azo dye in water by several oxidation processes – a comparative study. Dyes and Pigments. 2004; 60:61–68.

Nirmal M, Dabbousi BO, Bawendi MG, Macklin JJ, Trautman JK, Harris TD, Brus LE. Fluorescence intermittency in single cadmium selenide nanocrystals. Nature. 1996; 383:802–804.

Oberdorster G, Oberdorster E, Oberdorster J. nanotoxicology: An emerging discipline evolving from studies of ultrafine particles. Environ Health Perspect. 2006; 113:823–829. [PubMed: 16002369]

Pflücker F, Wendel V, Hohenberg H, Gartner E, Will T, Pfeiffer S, Wepf R, Gers-Barlag H. The human stratum corneum layer: an effective barrier against dermal uptake of different forms of topically applied micronised titanium dioxide. Skin Pharm Appl Skin Physiol. 2001; 14 (S1):92–97.

Pinaud F, Michalet X, Bentolila LA, Tsay JM, Doose S, Li JJ, Iyer G, Weiss S. Advances in fluorescence imaging with quantum dot bio-probes. Biomaterials. 2006; 27:1679–1687. [PubMed: 16318871]

Popov AP, Ledemann J, Priezzhev AV, Myllylä R. Effect of size of TiO_2 nanoparticles embedded into stratum corneum on ultraviolet-A and ultraviolet-B sun-blocking properties of the skin. J Biomed Opt. 2005; 10(6):064037, 1–9. [PubMed: 16409102]

Popov AP, Priezzhev AV, Ladermann J, Myllylä R. The effect of nanometer particles of titamium oxide on the protective properties of skin in the UV region. J Opt Technol. 2006; 73:208–211.

Rouse JG, Yang J, Ryman-Rasmussen JP, Barron AR, Monterio-Riviere NA. Effects of mechanical flexion on the penetration of fullerene amino acid-derivatized peptide nanoparticles. Nano Lett. 2007; 7:155–160. [PubMed: 17212456]

Ryman-Rasmussen JP, Riviere JE, Monterio-Riviere NA. Penetration of intact skin by quantum dots with diverse physicochemical properties. Toxicol Sci. 2006; 91:159–165. [PubMed: 16443688]

Schulz J, Hohenberg H, Pflücker F, Gärtner E, Will T, Pfeiffer S, Wepf R, Wendel V, Gers-Barlag H, Wittern KP. Distribution of sunscreens on skin. Adv Drug Deliv Rev. 2002; 54:S157–S163. [PubMed: 12460721]

Smith AM, Ruan G, Rhyner MN, Nie S. Engineering luminescent quantum dots for in vivo molecular and cellular imaging. Ann Biomed Eng. 2006; 34:3–14. [PubMed: 16450199]

Stevenson M, Bullock K, Lin W-Y, Rajeshwar K. Sonolytic enhancement of the bactericidal activity of irradiated titanium dioxide suspensions in water. Res Chem Intermed. 1997; 23:311–323.

Sunada K, Kikuchi Y, Hashimoto K, Fujishima A. Bactericidal and detoxification effects of TiO_2 thin film photocatalysts. Environ Sci Technol. 1998; 32:726–728.

Tan MH, Commens CA, Burnett L, Snitch PJ. A pilot study on the percutaneous absorption of microfine titanium dioxide from sunscreens. Australasian J Dermatol. 1996; 37:185–187.

Uren, RF.; Hoefnagel, CA. Lymphoscintigraphy. In: Thompson, JF.; Morton, DM.; Kroon, BBR., editors. Textbook of Melanoma. 1. Martin Dunitz, Taylor and Francis Group; London: 2004. p. 339-364.

Voura EB, Jaiswal JK, Mattoussi H, Simon SM. Tracking metastatic tumor cell extravasation with quantum dot nanocrystals and fluorescence emission-scanning microscopy. Nat Med. 2004; 10:993–998. [PubMed: 15334072]

Yu WW, Qu L, Guo W, Peng X. Experimental determination of the extinction coefficient of CdTe, CdSe, and CdS nanocrystals. Chem Mater. 2003; 15:2854–2860. [Erratum/Correction in *Chem. Mater.* 16(2004), 560].

Yu WW, Chang E, Falkner JC, Zhang J, Al-somali AM, Sayes CM, Johns J, Drezek R, Colvin VL. Journal of the American Chemical Society. 2007; 129(10):2781.

Wahi RK, Liu YP, Falkner JC, Colvin VL. Solvothermal Synthesis and Characterization of Anatase TiO2 Nanocrystals with Ultrahigh Surface Area. Journal of Colloid and Interface Science. 2006; 302 (2):530–536. [PubMed: 16889789]

Wahi RK, Yu WW, Liu YP, Meija ML, Falkner JC, Nolte W, Colvin VL. Photodegradation of Congo Red Catalyzed by Nanosized TiO_2. Journal of Molecular Catalysis – A- Chemical. 2005; 242(1–2):48–56.

Yu WW, Falkner JC, Shih BS, Colvin VL. Preparation and characterization of monodisperse PbSe nanocrystals in a non-coordinating solvent. Chem Mater. 2004a; 16:3318–3324.

Yu WW, Falkner JC, Yavuz CT, Colvin VL. Synthesis of monodisperse iron oxide nanocrystals by thermal decomposition or iron carboxylate salts. Chem Commun (Camb). 2004b; 2004:2306–2307.

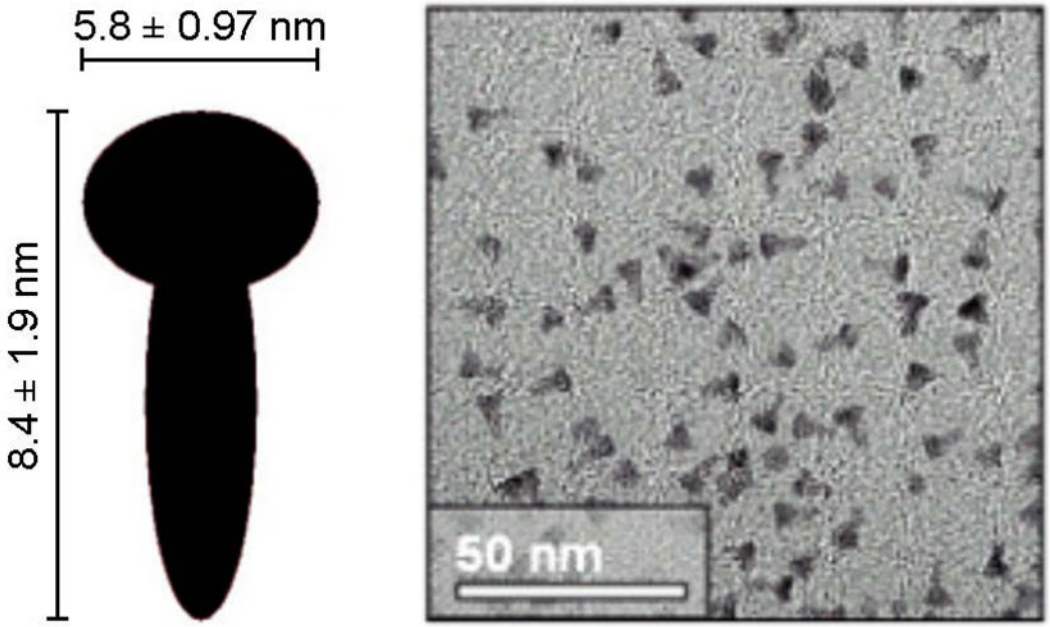

FIGURE 1.
Characterization of QD using TEM. The QD were characterized using TEM and the average QD CdSe core size was nail shaped with an 8.4 ± 1.92 nm length and 5.8 ± 0.97 nm width, resulting in an aspect ratio of 1.45.

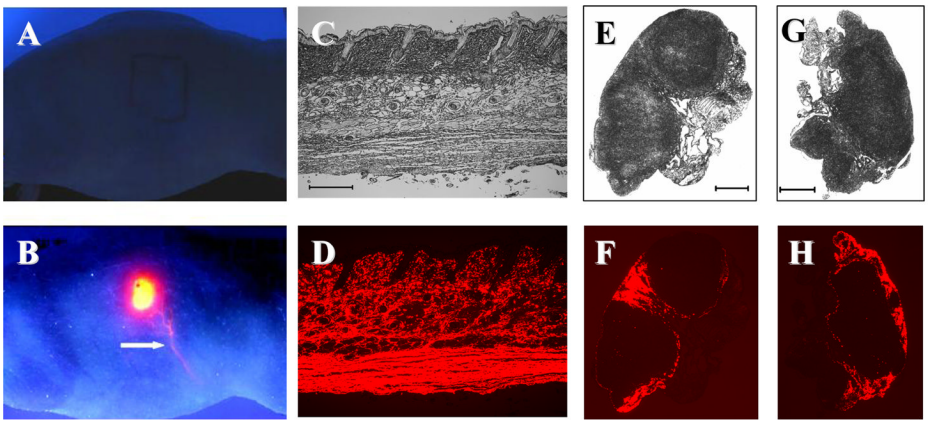

FIGURE 2.

Panels A,B: Female SKH-1 hairless mice were injected with 5 μL saline (A) or 5 μL of QD solution (B) and digital images were taken following ultraviolet-A illumination. The tracking of red fluorescent QD into the lymphatics is shown in the lower panel (arrow). **Panels C–H:** Twenty-four hours after injection, the mice were sacrificed, and the tissues were removed, preserved in formalin, and sectioned for microscopic examination. Bright field (panels C, E, G) and fluorescence (panels D, F, H) images were taken of intradermal injection site skin (panels **C, D**; bar = 200 μm), right axillary lymph node (panels **E, F**; bar = 500 μm), and right brachial lymph node (panels **G,H**; bar = 500 μm). The red fluorescent QD are visible in sections of the lymph nodes.

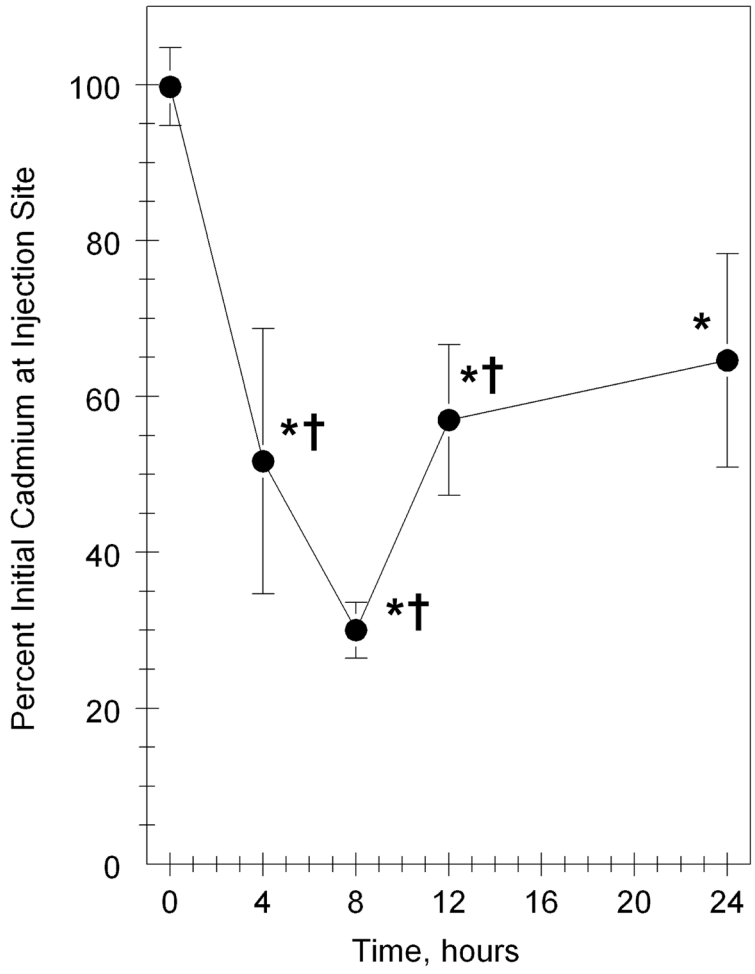

FIGURE 3.

The percent of the initial dose of cadmium that remained at the site of injection of the CdSe QD. The skin that contained the site of injection was removed, completely digested using HNO3, and the total cadmium was detected using ICP-MS (mean ± standard error). Values indicated by an asterisk (*) were significantly different (p 0.05) than the value at 0 hr, while values indicated with the cross (†) were not significantly different from each other (p>0.05).

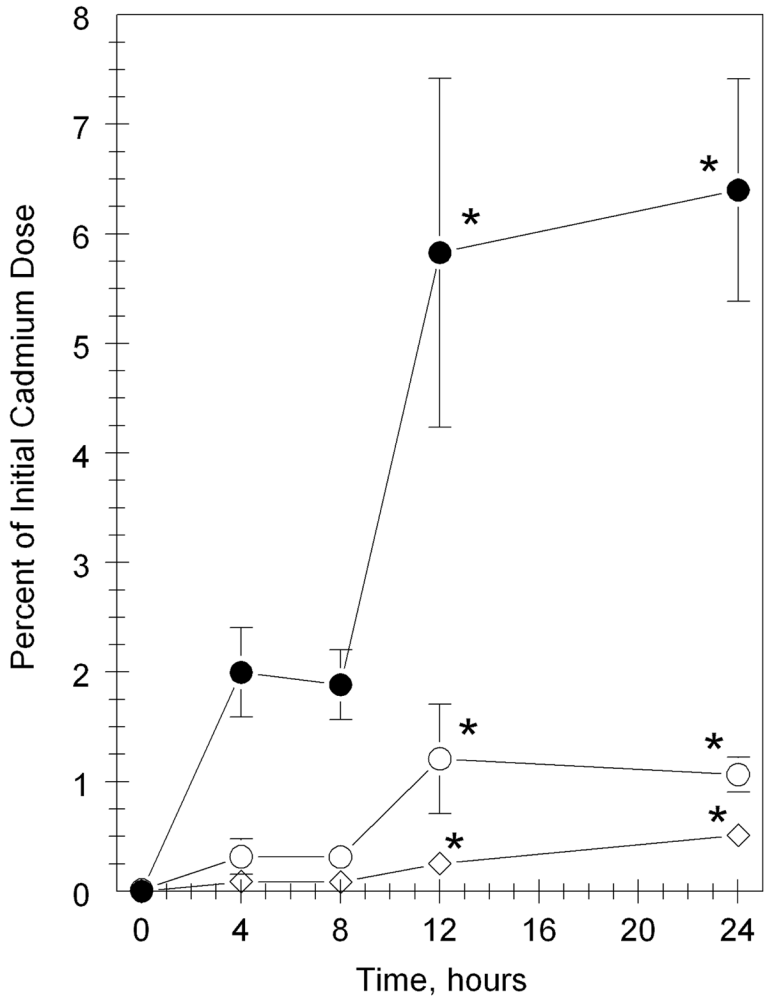

FIGURE 4.

Distribution of cadmium in organs following intradermal injection of CdSe QD. The data are expressed as mean ± standard error for: liver (solid circle); regional lymph nodes (open circle); kidney (open diamond). Values indicated by an asterisk (*) were significantly different ($p<0.05$) than the value in the same organ at 0 hr.

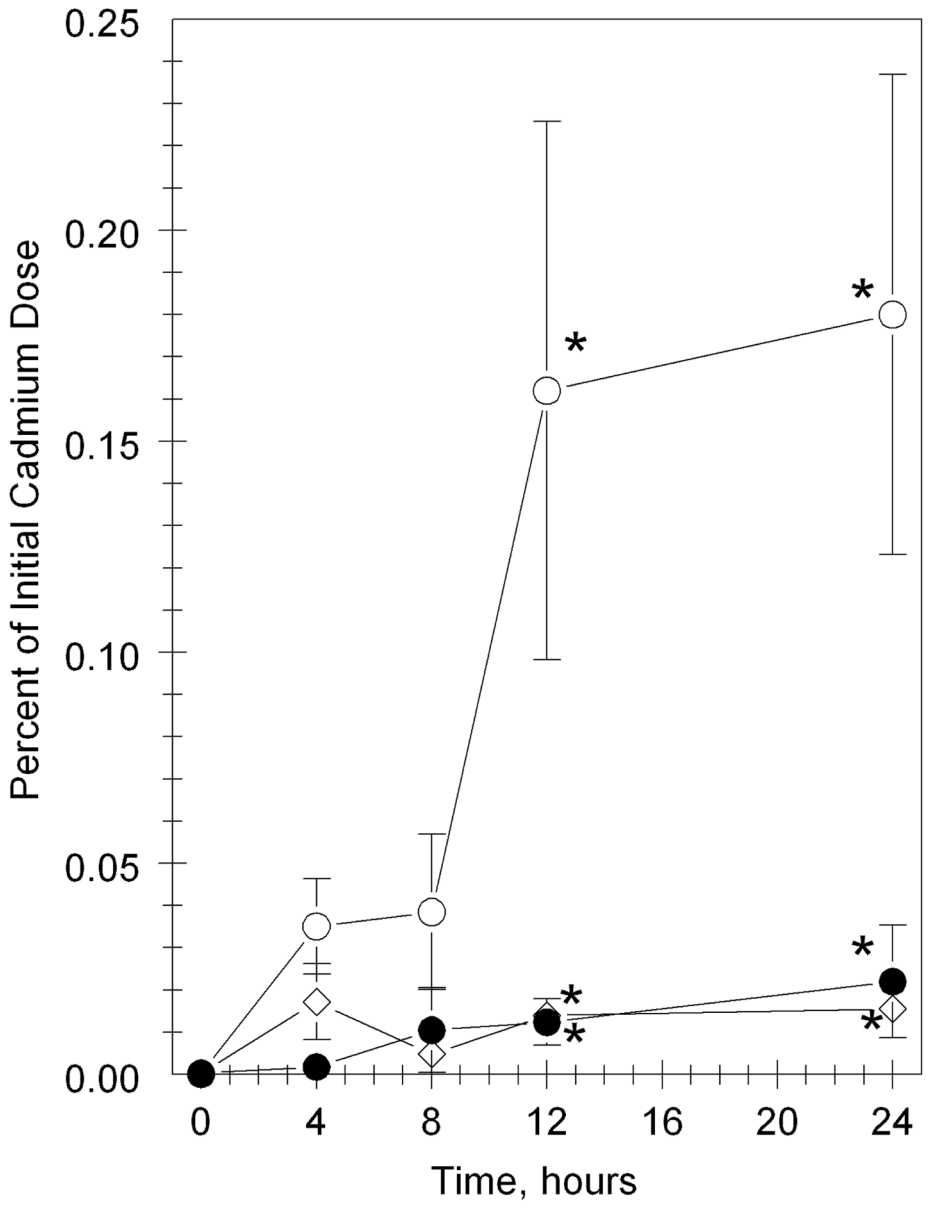

FIGURE 5.

Distribution of cadmium in organs following intradermal injection of CdSe QD. The data are expressed as mean ± standard error for: hepatic lymph node (solid circle); spleen (open circle); heart (open diamond). Values indicated by an asterisk (*) were significantly different ($p<0.05$) than the value in the same organ at 0 hr.